Received: 30 November 2020 | Revised: 23 March 2021 | Accepted: 15 April 2021

DOI: 10.1002/nbm.4535

RESEARCH ARTICLE

NMR IN BIOMEDICINE WILEY

Characterization of anisotropic T2W signals from human knee femoral cartilage: The magic angle effect on a spherical surface

Yuxi Pang

Department of Radiology, University of Michigan, Ann Arbor, Michigan, USA

Correspondence
Yuxi Pang, PhD, Department of Radiology, University of Michigan, 1500 E. Medical Center Dr., Ann Arbor, MI 48109-5030, USA.
Email: yuxipang@umich.edu

Funding information
Eunice Kennedy Shriver National Institute of Child Health & Human Development of the National Institutes of Health (NIH), Grant/Award Number: R01-HD-093626-02

Abstract

The aim of the current study was to propose a generalized magic angle effect (gMAE) function for characterizing anisotropic T2W signals of human knee femoral cartilage with a spherical surface in clinical studies. A gMAE model function $f(\alpha, \varepsilon)$ was formulated for an orientation-dependent (ε) transverse T_2 (i.e., $1/R_2$) relaxation in cartilage assuming an axially symmetric distribution (α) of collagen fibers. T2W sagittal images were acquired on an adult volunteer's healthy knee at 3 T, and ROI-based average signals $S(\varepsilon)$ were extracted from angularly and radially segmented femoral cartilage. Compared with the standard MAE (sMAE) functions in the deep (DZ, $\alpha = 0°$) and in the superficial (SZ, $\alpha = 90°$) zones, a general form of R_2 orientation-dependent function $f(\alpha, \varepsilon)$ was fitted to $S(\varepsilon)$, including an isotropic R_2 contribution (internal reference [REF]). Goodness of fit was evaluated by root-mean-square deviations (RMSDs). An *F*-test and a paired *t*-test were respectively used to assess significant differences between the observed variances and means, with statistical significance set to p less than .05. As a symmetric orientation-dependence function with a varying dynamic range, the proposed gMAE model outperformed the previous sMAE functions manifested by significantly reduced RMSDs in the DZ (0.239 ± 0.122 vs. 0.267 ± 0.097, $p = .014$) and in the SZ (0.183 ± 0.081 vs. 0.254 ± 0.085, $p < .001$). The fitted average angle α (38.5 ± 34.6° vs. 45.1 ± 30.1°, $p < .43$) and REF (5.092 ± 0.369 vs. 5.305 ± 0.440, $p < .001$) were smaller in the DZ than those in SZ, in good agreement with the reported collagen fibril microstructural configurations and the non-bound water contribution to R_2 in articular cartilage. In conclusion, a general form of the magic angle effect function was proposed and demonstrated for better characterizing anisotropic T2W signals from human knee femoral cartilage at 3 T in clinical studies.

KEYWORDS
anisotropic T2-weighted imaging, human knee femoral cartilage, magic angle effect, orientation-dependent transverse relaxation, residual dipolar interaction, spherical surface

Abbreviations used: ARCADE, anisotropic R_2 of collagen degeneration; DZ, deep zone; FOV, field of view; HR, high resolution; LFC, lateral femoral condyle; MAE, magic angle effect; MFC, medial femoral condyle; RDC, residual dipolar coupling; REF, internal reference; RMSD, root-mean-square deviation; ROI, region of interest; SENSE, sensitivity encoding; SZ, superficial zone; T2W, T2-weighted image; TE, echo time; TZ, transitional zone.

1 | INTRODUCTION

The magic angle effect (MAE) is a well-known phenomenon of anisotropic transverse T_2 (i.e., $1/R_2$) relaxation in MR imaging of highly ordered biological tissues such as tendons and articular cartilage,[1–3] yet its potential in unraveling physiological and pathological changes has not been fully exploited.[4,5] For tendons and cartilage, the MAE originates from some restricted water molecules buried inside collagen triple-helical microstructures,[6,7] manifested by residual dipolar coupling (RDC) between two water protons that is proportional to a spatial factor $\langle 3\cos^2\theta - 1\rangle$.[8–10] Herein, an internuclear dipolar interaction vector makes an angle θ relative to the static magnetic field B_0, and an ensemble or time average is represented by angle brackets. It should be mentioned that MAE does not exclusively belong to collagen, a major cable-like structural protein in the human body.[11] Regardless of distinct water-residing environments, MAE will appear whenever water molecular reorientations are somewhat hindered.[12–14] In an isotropic liquid solution, RDC will vanish due to unrestricted and rapid water molecular motions; on the other hand, the specific spatial factor $\langle 3\cos^2\theta - 1\rangle$ could also become zero in an anisotropic environment given that the relevant water molecules are orientated preferentially with $\theta = 54.7^\circ$, the so-called magic angle (MA).[3,8]

When the MA condition is fulfilled, an anisotropic transverse relaxation $R_2^a(\theta)$ in highly ordered biological tissues will disappear, resulting in the widely reported hyperintensity T_2-weighted images in the literature.[1,3] It is worthwhile to emphasize that $R_2^a(\theta)$ is determined by the variance of RDC, that is, $\langle(3\cos^2\theta - 1)^2\rangle$, rather than RDC itself.[9,10] For knee articular cartilage, R_2 could be conveniently categorized into isotropic R_2^i and anisotropic $R_2^a(\theta)$ components,[9,10,15] with the latter specifically associated with the integrity of collagen fibril ultrastructures.[4,5,16] With respect to other relaxation metrics that have been studied to date, R_2 is reportedly the most susceptible to orientation anisotropy, but with the best sensitivity in detecting early degenerations in cartilage due to osteoarthritis.[4] If the isotropic component had been removed from R_2, the resulting R_2, that is, $R_2^a(\theta)$, would have possessed markedly improved specificity in revealing biochemical and microstructural changes well before visible morphologic alterations.[17–19] Unfortunately, R_2^i and $R_2^a(\theta)$ are not commonly separated from each other in conventional R_2 mapping in clinical studies of human knee articular cartilage.

Recently, an efficient $R_2^a(\theta)$ mapping method, referred to as ARCADE,[20] has been proposed based on a single T2W sagittal image, in which an internal reference (REF) is exploited for separating $R_2^a(\theta)$ from its counterpart R_2^i in human knee femoral cartilage at 3 T. This particular REF must be deduced from the MA orientation of collagen fibers in the deep zone (DZ), by fitting the standard magic angle effect (sMAE) function, that is, $\langle(3\cos^2\theta - 1)^2\rangle$, to angularly segmented T2W signals. Surprisingly, it was found that the commonly used sMAE function was only adequate for characterizing a few sagittal imaging slices.[20] The reliability of the determined REF could have been markedly improved if it had been derived from more imaging slices than otherwise used.

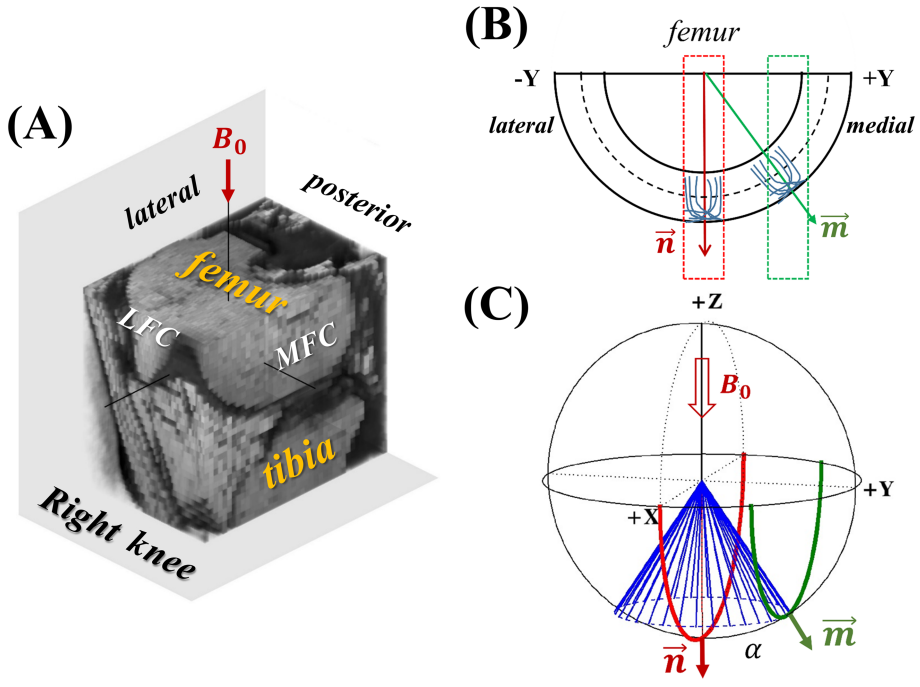

FIGURE 1 A partial volume-rendered high-resolution image of an adult human right knee (A). Two schematic sagittal imaging slices cutting through one femoral condyle's center (red) and off-center (green) in two-dimensional (coronal view) (B) and three-dimensional (unit sphere) diagrams (C) assuming a spherical surface of cartilage. LFC, lateral femoral condyle; MFC, medial femoral condyle

As illustrated in Figure 1A, human knee femoral cartilage has a curved surface because of two extruding condyles, that is, lateral (LFC) and medial (MFC) femoral condyles,[21,22] which could be approximately described by a spherical surface. Even although a circle could be defined for the angularly segmented femoral cartilage in a sagittal imaging plane,[20,21,23] the normal vector ($\vec{m}$) to cartilage surface imaged in a lateral or medial slice (green box) will deviate from those ($\vec{n}$) imaged close to the central condyles (red box), as depicted schematically in a coronal plane (Figure 1B) and a unit sphere (Figure 1C). These unusual locations of off-center imaging slices are not compatible with what has been typically assumed in the sMAE function, in which the cartilage surface normal could be parallel along B_0 and within the imaged sagittal slice. Without taking into account the fact that the femoral cartilage has an irregular surface, some previously reported clinical R_2 anisotropy measurements would have appeared to be contradictory with the well-established MAE.[23,24]

On the other hand, the collagen fibril microstructural distributions from the uppermost (i.e., cartilage surface) to the innermost layers of articular cartilage are extremely complex.[25,26] In the past, various models have been developed for characterizing the detailed fibril architectures in both the animal and the human tissues. In a microscopy MR imaging (μMRI) 7-T study of canine humeral heads at an extremely high resolution,[26] three models (i.e., solid cone, funnel and fan) of fibril configurations were extensively investigated, and the collagen fibril distributions in the superficial zone (SZ) were reportedly better characterized by a combination of the first two models while the third model was the choice for those in the DZ. In another prior T2W study on healthy human knees at 7 T,[27] the solid cone model was also used for quantifying the depth-dependent anisotropic cartilage architecture. Unlike the previously reported ex vivo study,[26] an analytical function for the solid cone model was provided; but this specific function became valid only within a limited orientation range for fibril distributions from the DZ to the transitional (TZ) zone. In other words, this particular model was not suitable for quantifying collagen microstructures in the SZ of human knee articular cartilage.

In clinical 3-T studies of orientation-dependent T2W imaging of human knee femoral cartilage, two halves of cartilage layers (i.e., the DZ and the SZ) are usually partitioned due to a limited imaging resolution, as shown schematically in Figure 2B.[20,23] It should be pointed out that the segmented DZ most likely includes multiple layers with fibril microstructures orientated differently from $\vec{n}$, and the segmented SZ covers at least both the histologically defined SZ and TZ of the femoral cartilage,[28,29] as illustrated in Figure 2A, where the collagen fibril histological distributions diverge continuously from the DZ to the SZ based on the well-known arcade model,[30,31] and are further depicted by the funnel model using different α angles.[26]

While T2W anisotropies in an ideal DZ or SZ layer could be respectively characterized by the sMAR function of $(3\cos^2\theta - 1)^2$ or $(1 - 3\sin^2\theta + (27/8)\sin^4\theta)$,[9,30] a general form of the magic angle effect (gMAE) function must be sought to quantify realistic fibril microstructural

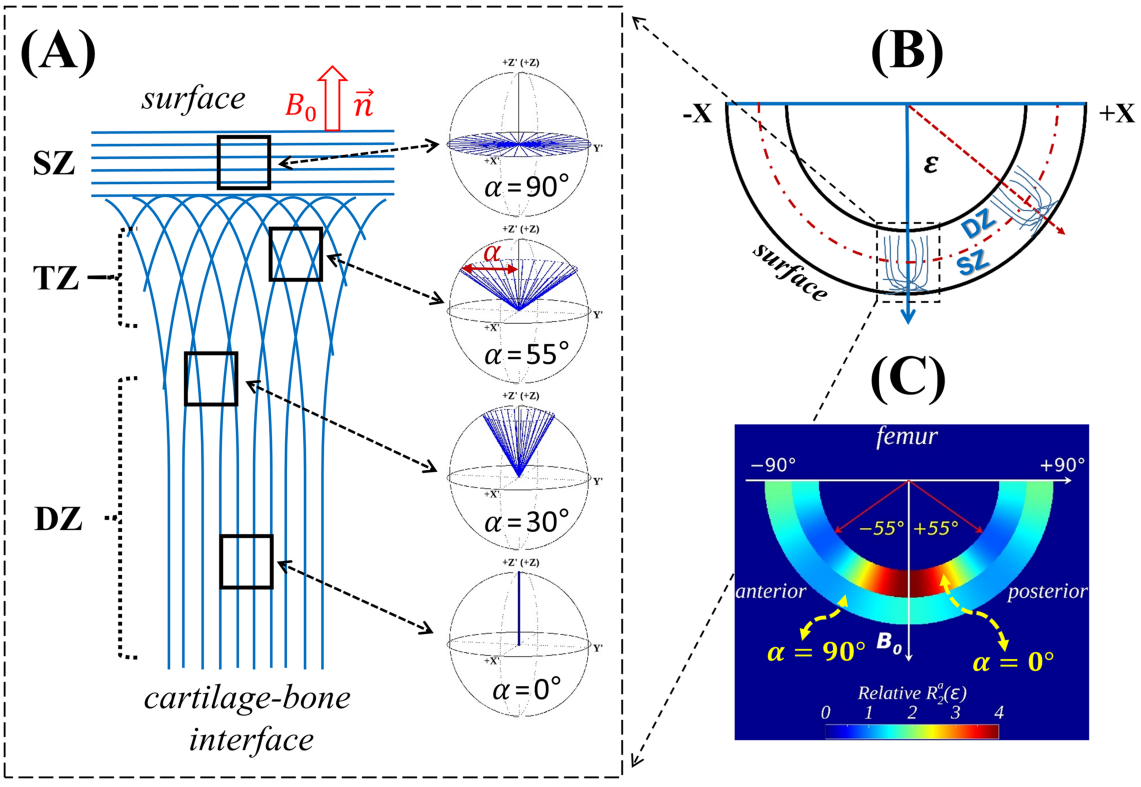

FIGURE 2 Schematics of two-dimensional arcade and three-dimensional funnel models with varying collagen fibril distributions (A) taken from an ideal sagittal imaging slice (B) exhibiting characteristic R_2 orientation-dependences in two segmented cartilage zones (C). DZ, deep zone; SZ, superficial zone; TZ, transitional zone

configurations in angularly segmented femoral DZ and SZ cartilage on a curved surface. To better characterize anisotropic T2W images of human knee articular cartilage from clinical studies and derive a less biased REF and thus a reliable anisotropic R_2 relaxation metric independent of T2W pulse sequences,[20] the curved nature and multiple-layer aspect in the femoral cartilage ought to be considered in the conventional MAE model. Therefore, this work aimed to propose a theoretical gMAE framework to meet an unmet need and demonstrate its performance on an asymptomatic knee of one adult volunteer at 3 T, with respect to the commonly used sMAE models.

2 | METHODS

2.1 | Theory

Water proton intramolecular dipolar interactions in collagen-rich tissues are, on average, along the fiber bundles' primary direction.[6,7,9] With respect to the surface normal ($\vec{n}$) in cartilage, the collagen fibril microstructures are, as depicted in Figure 2A, predominantly orientated perpendicularly, at random and in parallel in the SZ, TZ and DZ, respectively.[29,30] Given an image voxel comprising the fibril microstructures distributed in an axially symmetric system when $\vec{n}$ is not aligned with B_0, as shown in Figure 3A,[9,26] the orientation dependence of an anisotropic transverse relaxation $R_2^a(\theta)$ of water protons in cartilage can be derived from an ensemble average of dipolar interactions associated with differently orientated fibers, that is, $\langle(3\cos^2\theta - 1)^2\rangle$.

In this oversimplified symmetric model, an exact distribution of collagen fibers could be adequately characterized by two constant angles α and ε, along with two varying angles θ and φ. Specifically, a representative fiber forms an angle α with $\vec{n}$ that, in turn, makes an angle ε with B_0. An angle θ is formed between the fiber and B_0, and an angle φ is an azimuthal angle of the fiber ranging from 0 to 2π. To evaluate an orientation (i.e., θ) dependence function in terms of angles α and ε, that is, $f(\alpha,\varepsilon) = \langle(3\cos^2\theta - 1)^2\rangle$, the term cos θ has to be recast using other trigonometric forms containing α, ε and φ, and an ensemble average has to be taken over all φ angles.

According to the spherical law of cosines, the term cos θ can be expressed by $(\cos\alpha\cos\varepsilon+\sin\alpha\sin\varepsilon\cos\varphi)$. As a result, the subfunction of $(3\cos^2\theta - 1)$ could be represented by a three-termed expression, that is, $(1/2)(3\cos^2\alpha - 1)(3\cos^2\varepsilon - 1)+(3/2)\sin^2\alpha\sin^2\varepsilon\cos2\varphi$ + (3/2)

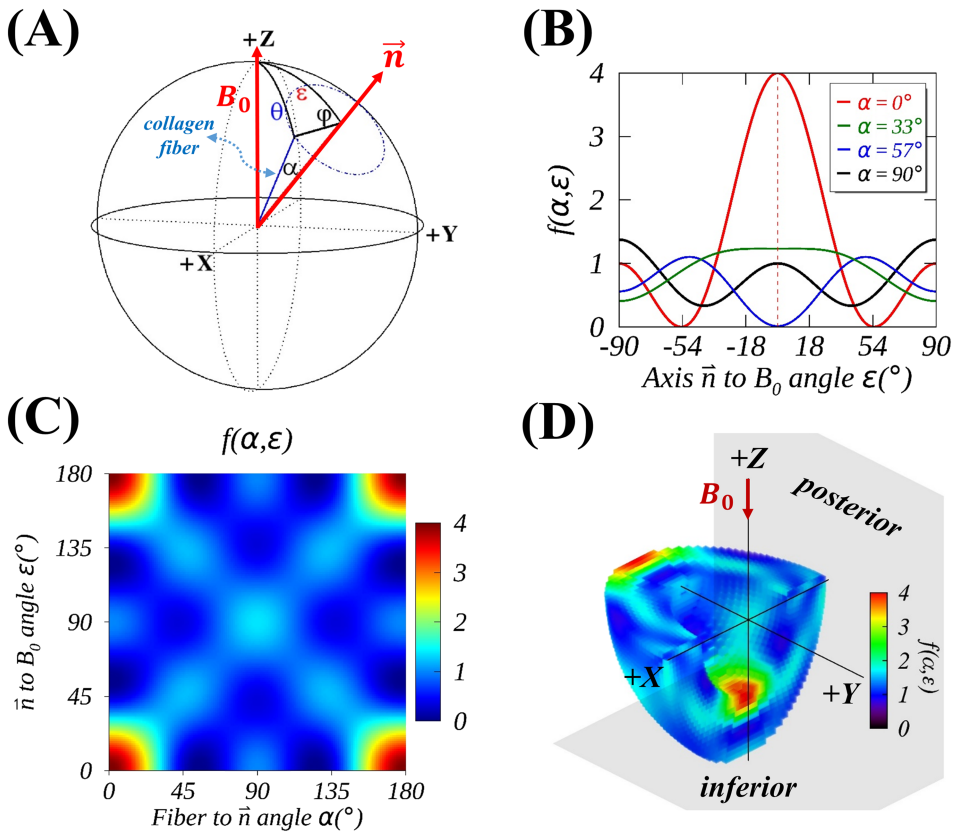

FIGURE 3 An axially symmetric model (A) for collagen fibril distributions with cartilage surface normal denoted by $\vec{n}$. An orientation-dependent function $f(\alpha,\varepsilon)$ is depicted by four line profiles (B) with $\alpha = 0°$ (red), 33° (green), 57° (blue) and 90° (black), by a 2D map (C) with $\alpha = \varepsilon = 0$–180°, and by a multiple ($n = 11$) layers quarter-sphere (D) with $\alpha = 0$–90° from the innermost to outermost layers

$\sin2\alpha\sin2\varepsilon\cos\varphi$.[32] After this subfunction has been squared then an ensemble average taken, $f(\alpha,\varepsilon)$ could be simply expressed by Equation 1. It should be noted that all trigonometric terms containing either $\langle\cos\varphi\rangle$ or $\langle\cos2\varphi\rangle$ become zero.

$$f(\alpha,\varepsilon)=(1/4)\left\{\left(3\cos^2\alpha-1\right)^2\left(3\cos^2\varepsilon-1\right)^2\right\}+(9/8)\left\{(\sin\alpha\sin\epsilon)^4+(\sin2\alpha\sin2\epsilon)^2\right\}. \quad (1)$$

Even although it appears markedly different from what has been presented in his seminal paper by Berendsen,[9] $f(\alpha,\varepsilon)$ will give the same orientation dependence, except for a scaling factor of 9/4. This axially systematic model was referred to as the funnel model in the literature but without an analytical function.[26] When $\alpha = 0^\circ$ and 90°, $f(\alpha,\varepsilon)$ will restore the sMAE functions previously used in the DZ and SZ, respectively.[30]

One salient feature of $f(\alpha,\varepsilon)$ is that its multitude symmetries originated from the characteristics of an axially symmetric model, as revealed in both Equation 1 and Figure 3C. Accordingly, the observed orientation dependence could be interpreted as α variations while keeping ε constant, and vice versa. As shown in Figure 1A, the femoral cartilage has a curved surface, and it is infrequent for the surface normal to be parallel to B_0 in standard sagittal images. From angularly segmented ROIs, an orientation-dependent form can always be derived regardless of its association with the surface normal, as schematically demonstrated for one imaging slice (green) in Figure 1C.

When an imaging slice deviates from the center of the femoral condyles, its surface normal $\vec{m}$ will make an angle α with $\vec{n}$ from the central slice when $\varepsilon = 0$, assuming that the femoral condyle has an ideally half-sphere shape. Mathematically, it is indistinguishable between $f(\alpha,\varepsilon)$ and $f(\varepsilon,\alpha)$; as a result, it is appropriate to quantify the orientation dependences (ε) for all imaging slices with an adjustable parameter α to account for the differences, not only in sagittal slice locations but also in fibril architectures across the femoral cartilage layers.

2.2 | T2W MR imaging of human knee cartilage

T2W sagittal images were acquired using an interleaved multislice ($n = 32$) multiecho ($n = 8$) turbo spin echo sequence, with a 16-channel T/R knee coil on an Ingenia 3-T MR scanner (Philips Healthcare, Best, The Netherlands). Some key acquisition parameters were listed as follows: field of view (FOV) = 128 x 128 x 96 mm^3; acquired/reconstructed voxel size = 0.6 x 0.6 x 3.0/0.24 x 0.24 x 3.0 mm^3; compressed SENSE[33] factor = 2.5; image readout bandwidth = 443.3 Hz; TR = 2500 ms; TEs = n x 6.1 ms with n = 1–8; and total scan time = 7 min 25 s. In this study, only T2W images with a TE of 48.8 ms were evaluated from the asymptomatic right knee of one consenting male subject (aged 35 years) in an internal review board (IRB)-approved clinical study.

A high-resolution (HR) 3D image of the same knee was also acquired using the turbo spin echo sequence with a variable flip angle excitation scheme. The FOV was 129 x 129 x 129 mm^3 and the acquired voxel size was 0.52 x 0.52 x 0.52 mm^3, which was then interpolated to 0.26 x 0.26 x 0.26 mm^3. An effective TE and TR were 37 and 1000 ms, respectively. With a compressed SENSE reduction factor of 3, the total scan time was 5 min 6 s. This HR dataset was used only for visualization purposes in the current study.

2.3 | Angular and radial segmentations

The femoral cartilage was first manually delineated on each of the T2W sagittal imaging slices using the free software ITK-SNAP.[34] Next, a large circle was fitted to the whole femoral cartilage, from which angularly segmented ROIs were partitioned with an angular resolution of 5°, each with an estimated angle β relative to B_0, which pointed downward in the image (Figure 4). These estimated β angles, which were assumed to be aligned with the varying normal vectors on the curved cartilage surface, were further refined based on locally defined circles using only adjacent ($\beta \pm 10^\circ$) spatial information to better represent the normal vector ($\vec{n}$) in the femoral cartilage.[20] Finally, these angularly segmented ROIs were further subdivided into the DZ and SZ equally in the radial direction.

2.4 | Modeling anisotropic T2W signals

An average T2W signal intensity, S, from one segmented ROI in femoral cartilage, could be conveniently expressed by Equation 2 as follows,

$$S = S_0\exp\left\{-\left(R_2^i + R_2^a \times f(\alpha,\varepsilon)\right)TE\right\} \quad (2)$$

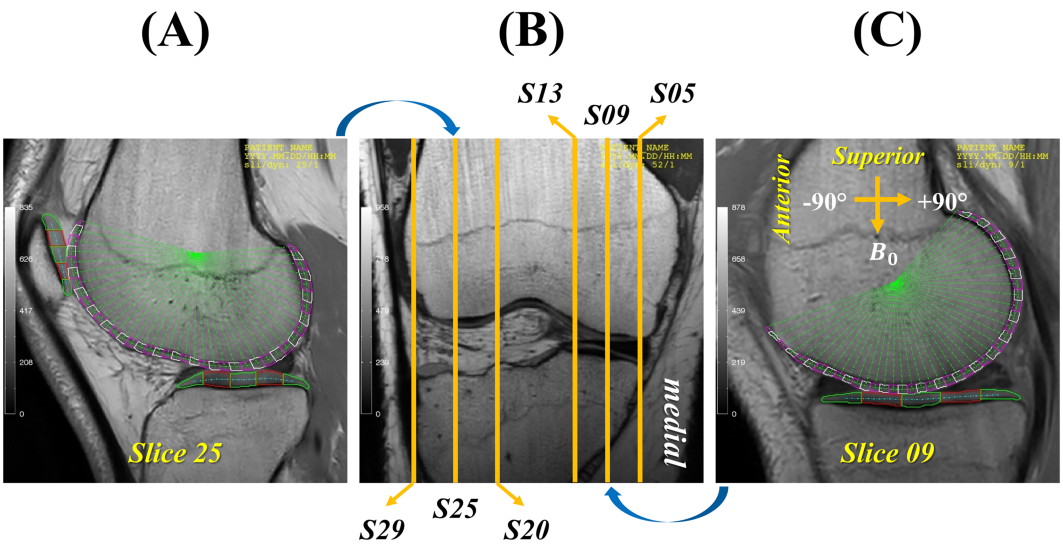

FIGURE 4 A high-resolution coronal image of an adult human right knee (B) with labeled locations for acquired sagittal imaging slices from lateral (slices 20, 25 and 29) and medial (slices 05, 09 and 13) femoral condyles. The sagittal images of central slices 25 (A) and 09 (C) are displayed with angularly and radially segmented ROIs superimposed

where S_0, R_2^i, R_2^a x $f(\alpha, \varepsilon)$ and TE represent initial signal intensity when TE = 0, isotropic and anisotropic R_2, and the echo time, respectively. On a logarithmic scale, Equation 2 was transformed into Equation 3, which was the anisotropic R_2 model used to fit the segmented orientation-dependent data from any imaging slices.

$$y(\varepsilon) = A - B \text{x} f(C, \varepsilon), \tag{3}$$

For this particular anisotropic R_2 model, ε was an independent variable and the three fitted model parameters were as follows: $A = \left(Log\, S_0 - R_2^i \times TE\right)$, also called a REF in the literature[20]; $B = R_2^a$ x TE; and $C = \alpha$. Once a global REF was determined, an anisotropic R_2 could be calculated simply as $(A - \log S)/TE$, as demonstrated before using a single T2W image.[20] Clearly, when a REF was underestimated, so too would be the derived anisotropic R_2, thereby increasing the possibility of becoming nonphysical negative relaxation values. For comparative purposes, the three-parameter data fitting using Equation 3 was labeled as "gMAE" for both the DZ and SZ data, whereas the two-parameter fitting for both the DZ ($C = 0°$) and SZ ($C = 90°$) data were referred to as "sMAE".

2.5 | Nonlinear least-squares fitting

Data modeling was performed by minimizing the total χ^2 value, defined as the sum of squared deviates between the modeled and the measured data. These residuals had been normalized by the corresponding measurement uncertainties (i.e., 1-σ standard deviations). The χ^2 minimization was accomplished using a publicly available IDL script (http://purl.com/net/mpfit) based on the Levenberg–Marquardt technique for nonlinear least-squares curve fitting.[35] During the χ^2 optimization processes, the fitting parameters were constrained as follows: $A = [3, 7]$; $B = [0.01, 2]$ and $C = [0, 90°]$, with the first two determined heuristically. The maximum number of iterations was limited to 200 for one set of initial values of fitting parameters within their constraints, and five sets of different starting values were used to prevent from being trapped into the local minima.[36]

The root-mean-square deviation (RMSD) was calculated as a measure of goodness of fit. An F-test was performed to assess the statistical significance of the goodness of fit, based on the RMSD calculated from two models. A p value was then derived from F-distribution, with significance indicated by p less than .05. Additionally, a paired t-test was used with significance set to p less than .05, assessing the mean differences between two fitted parameters. All image and data analysis were completed with customized software developed in IDL 8.5 (Harris Geospatial Solutions, Inc., Broomfield, CO, USA). Unless indicated otherwise, all the fitted data are presented as mean ± standard deviation.

3 | RESULTS

3.1 | Theoretical anisotropic R_2 orientation-dependence $f(\alpha, \varepsilon)$

Figure 3B-D present $f(\alpha, \varepsilon)$ as four characteristic profiles (B) with $\alpha = 0°$ (red), 33° (green), 57° (blue) and 90° (black), a 2D distribution map (C), and a 3D multiple ($n = 11$) layers quarter-sphere (D) with α ranging from 0° (innermost) to 90° (outermost). An ideal imaging slice (i.e., XZ plane at Y = 0, with only two layers) is depicted in Figure 2C, showing the expected femoral cartilage R_2 orientation-dependence $f(0°, \varepsilon)$ and $f(90°, \varepsilon)$ in the DZ and SZ, respectively.

Some prominent features of $f(\alpha, \varepsilon)$ deserve mentioning. First, the dynamic range of $f(\alpha, \varepsilon)$ is markedly different depending on α. For instance, $f(0°, \varepsilon)$ has the largest range spanning from 0 ($\varepsilon = 54.7°$) to 4 ($\varepsilon = 0°$); on the other hand, it becomes hardly orientation-dependent when ε changed from 0° to 50° with $\alpha = 33°$ (Figure 3B). Second, the MA for $f(\alpha, \varepsilon)$ will magically disappear when $\alpha \neq 0°$, that is, $f(\alpha, \varepsilon) \neq 0$. Third, the multitude symmetries of $f(\alpha, \varepsilon)$ manifest that $f(\alpha, \varepsilon) = f(\alpha, \varepsilon \pm 180°)$, $f(\alpha, 90° - \varepsilon) = f(\alpha, 90° + \varepsilon)$, and $f(\alpha, \varepsilon) = f(\varepsilon, \alpha)$, as demonstrated in Figure 3C.

3.2 | Modeling T2W signals of femoral cartilage

A regional volume-rendered HR right knee is shown in Figure 1A, highlighting the curved nature of cartilage surfaces from the MFC and the LFC. Figure 4B pinpoints the spatial locations on an HR coronal image of six representative T2W sagittal images from the MFC (S05, S09 and S13) and the LFC (S20, S25 and S29). Two sagittal imaging slices approximately cutting through the central condyles are presented in Figure 4A (S25) and 4C (S09), with the angularly and radially segmented ROIs superimposed.

Figure 5 depicts the exemplary MFC image slices (first column), that is, slices 05 (5A), 09 (5B, Figure 4C) and 13 (5C), with the measured (black circles) and fitted (gMAE, solid red lines; sMAE, dashed green lines) segmented T2W signals in the DZ (second column) and SZ (third column). Similarly, Figure 6 demonstrates the three LFC image slices, that is, slices 20 (6A), 25 (6B, Figure 4A) and 29 (6C), and fitting results. Table 1 lists the resulting fitted parameters of these six representative imaging slices.

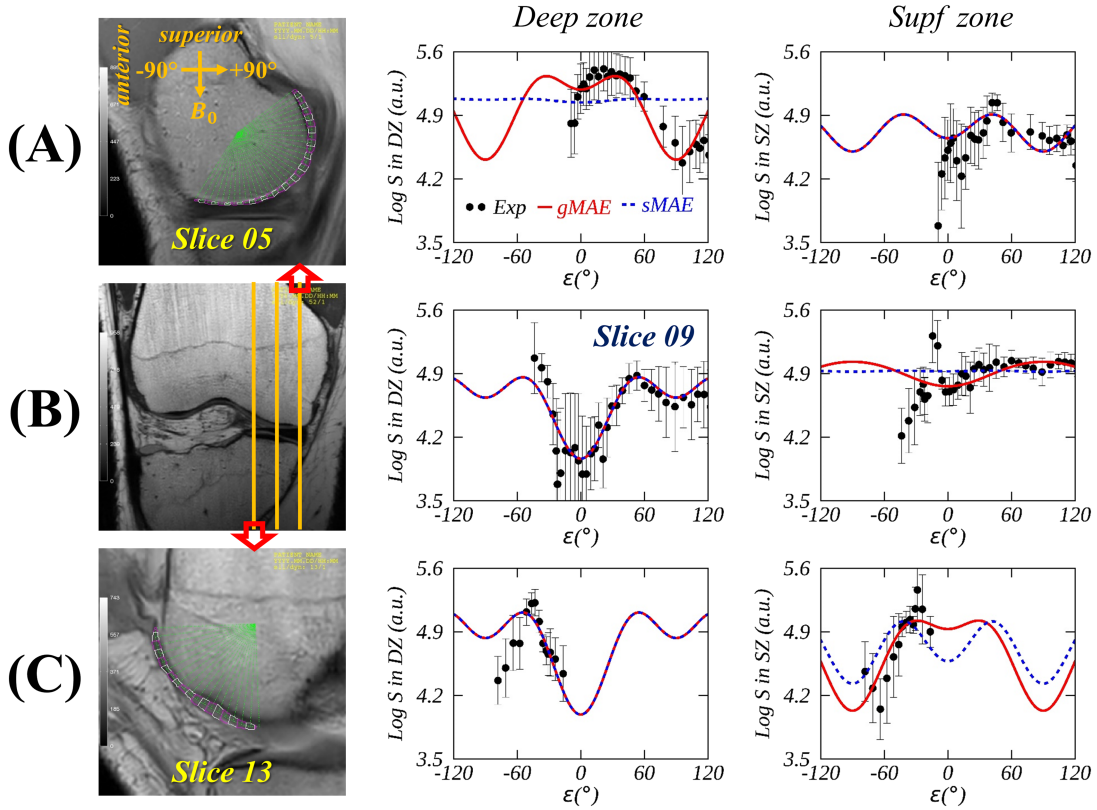

FIGURE 5 Measured (black circles) and fitted (generalized magic angle effect [gMAE], solid red lines; standard magic angle effect [sMAE], dashed blue lines) average T2W signal intensities in the deep (second column) and superficial (*Supf*) zones (third column) for slices 05 (A), 09 (B, Figure 4C) and 13 (C) from medial knee cartilage (first column)

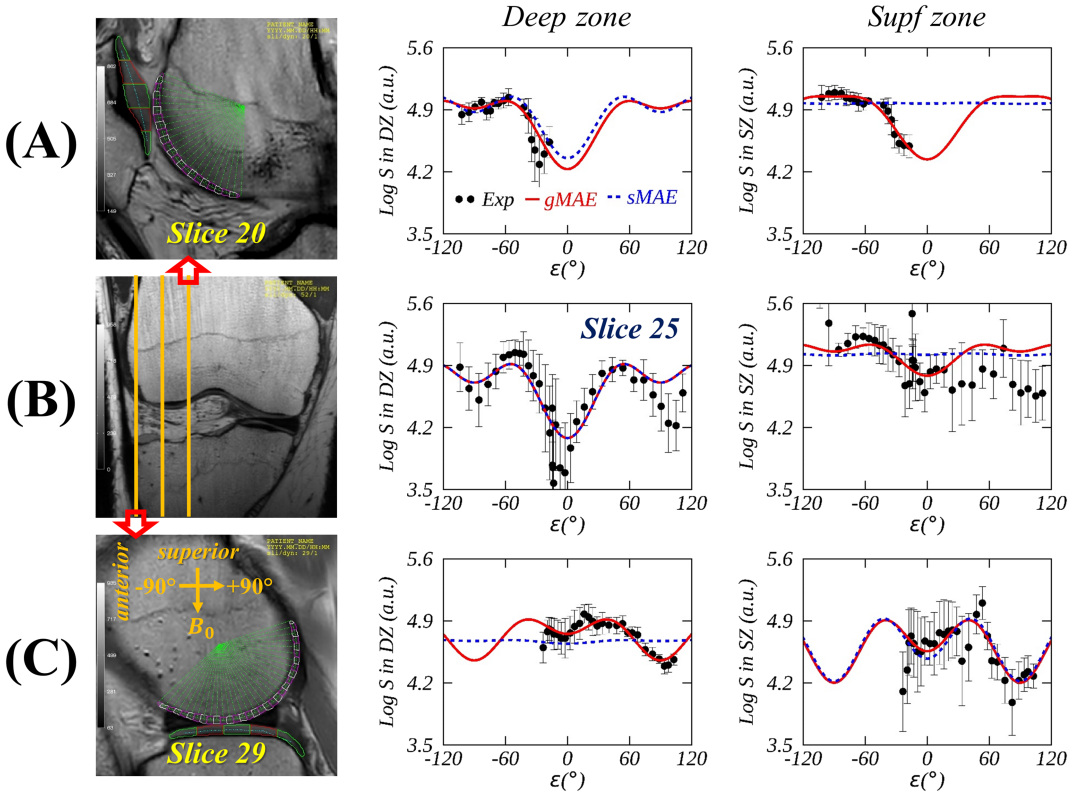

FIGURE 6 Measured (black circles) and fitted (generalized magic angle effect [gMAE], solid red lines; standard magic angle effect [sMAE], dashed blue lines) average T2W signal intensities in the deep (second column) and superficial (*Supf*) zones (third column) for slices 20 (A), 25 (B, Figure 4A) and 29 (C) from lateral knee cartilage (first column)

TABLE 1 Fitted model parameters, *A* (a.u.), *B* (a.u.) and α (°), from segmented T2W signal profiles in Figures 5 and 6 for the deep (DZ) and superficial (SZ) zones of the femoral cartilage from one adult subject's healthy knee

		gMAE				sMAE			
Slice index	Zone	A	B	α (°)	RMSD	A	B	RMSD	*p*
5	*DZ*	*6.13 ± 0.20*	*1.52 ± 0.28*	*75 ± 1*	*0.183*	*5.08 ± 0.05*	*0.01 ± 0.00*	*0.356*	*.001*
	SZ	*5.04 ± 0.15*	*0.39 ± 0.18*	*90 ± 5*	*0.283*	*5.04 ± 0.08*	*0.39 ± 0.10*	*0.283*	*1.000*
9	*DZ*	*4.86 ± 0.07*	*0.22 ± 0.05*	*0 ± 0*	*0.233*	*4.86 ± 0.07*	*0.22 ± 0.05*	*0.233*	*1.000*
	SZ	*5.14 ± 0.08*	*0.24 ± 0.09*	*30 ± 2*	*0.203*	*4.94 ± 0.02*	*0.01 ± 0.00*	*0.225*	*.760*
13	*DZ*	*5.11 ± 0.07*	*0.28 ± 0.07*	*0 ± 0*	*0.246*	*5.11 ± 0.07*	*0.28 ± 0.07*	*0.246*	*1.000*
	SZ	*5.95 ± 0.32*	*1.74 ± 0.51*	*74 ± 1*	*0.198*	*5.24 ± 0.13*	*0.66 ± 0.26*	*0.305*	*.148*
20	*DZ*	*5.15 ± 0.06*	*0.36 ± 0.10*	*21 ± 2*	*0.121*	*5.05 ± 0.04*	*0.17 ± 0.05*	*0.170*	*.297*
	SZ	*5.31 ± 0.06*	*0.50 ± 0.07*	*27 ± 1*	*0.054*	*4.98 ± 0.02*	*0.01 ± 0.00*	*0.229*	*.000*
25	*DZ*	*4.92 ± 0.04*	*0.21 ± 0.03*	*0 ± 0*	*0.251*	*4.92 ± 0.04*	*0.21 ± 0.03*	*0.251*	*1.000*
	SZ	*5.15 ± 0.08*	*0.10 ± 0.09*	*11 ± 17*	*0.295*	*5.04 ± 0.09*	*0.02 ± 0.10*	*0.307*	*.916*
29	*DZ*	*5.22 ± 0.07*	*0.64 ± 0.09*	*77 ± 1*	*0.50*	*4.68 ± 0.02*	*0.01 ± 0.00*	*3.90*	*.000*
	SZ	*5.25 ± 0.18*	*0.82 ± 0.22*	*81 ± 2*	*0.205*	*5.15 ± 0.14*	*0.68 ± 0.15*	*0.209*	*.820*

Abbreviations: gMAE, generalized magic angle effect; RMSD, root-mean-square deviation; sMAE, standard magic angle effect.

In general, gMAE provided significantly ($p < .01$) better fits for the edged imaging slices compared with sMAE, for instance, for slices 05 and 29 in the DZ, and slice 20 in the SZ. Compared with those changes between the DZ and the SZ from the central imaging slices, the observed T2W signal fluctuations from the edged slices appeared either more similar to (e.g., slice 20) or even reversed from each other (e.g., slice 29), signifying the curved nature of the femoral cartilage when deviated from the central condyles. These observations were in good agreement with the theoretical predictions, as shown in Figure 3.

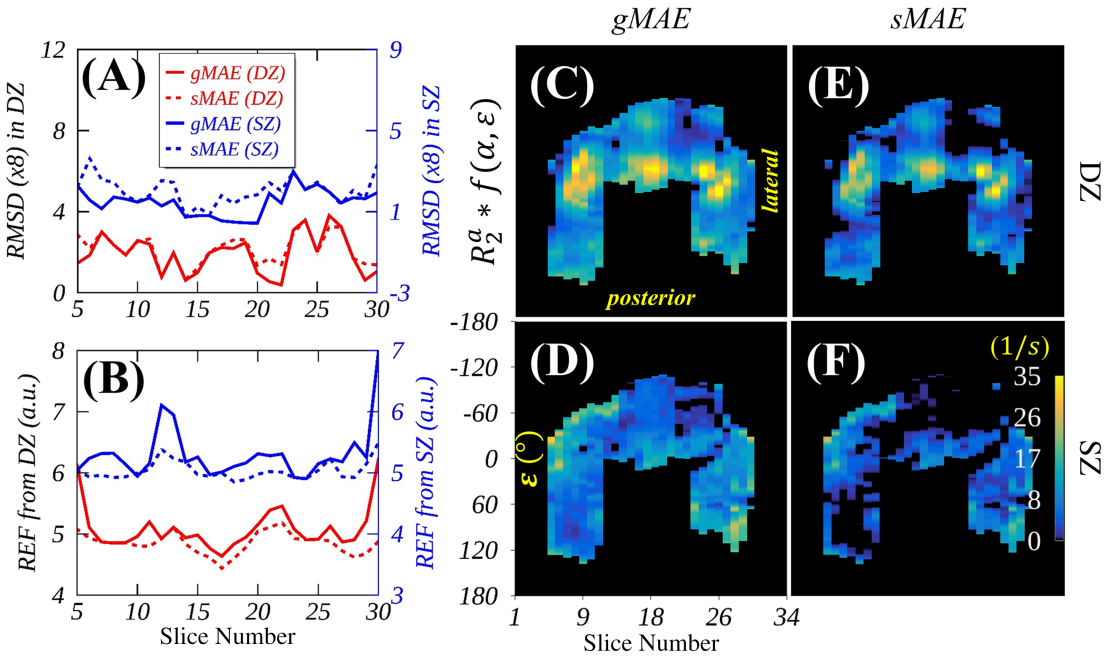

FIGURE 7 Comparisons of the root-mean-square deviations (RMSDs in A) and the fitted model parameter *A* (internal reference [REF] in B) for all imaging slices between generalized magic angle effect (gMAE; solid lines) and standard magic angle effect (sMAE; dashed lines) in the deep zone (DZ; red) and superficial zone (SZ; blue). Anisotropic R_2 parametric maps are shown using averaged REFs from gMAE (C and D) and sMAE (E and F) in the DZ (C and E) and SZ (D and F)

As demonstrated by the RMSDs of the fits for all the imaging slices in Figure 7A, gMAE on average significantly outperformed sMAE in the DZ (0.239 ± 0.122 vs. 0.267 ± 0.097, $p = .014$) and in the SZ (0.183 ± 0.081 vs. 0.254 ± 0.085, $p < .001$). Comparing gMAE with sMAE (Figure 7B), the fitted parameter *A* (i.e., REF) was significantly larger in the DZ (5.092 ± 0.369 vs. 4.850 ± 0.177, $p < .001$) and in the SZ (5.305 ± 0.440 vs. 5.035 ± 0.155, $p < .001$). In addition, a relatively smaller average angle α was observed in the DZ compared with that in the SZ (i.e., 38.5 ± 34.6° vs. 45.1 ± 30.1°, $p < .43$), which is largely consistent with the reported fibril microstructural arrangements from the DZ to the SZ in articular cartilage.[3,27]

When taking an average fitted *A* from both DZ and SZ as a global REF, the derived anisotropic R_2 maps of the femoral cartilage are presented in Figure 7C,D using gMAE fitting and in Figure 7E,F using sMAE fitting, in both the DZ (Figure 7C,E) and SZ (Figure 7D,F). When gMAE was compared with sMAE fitting, a relatively larger REF (i.e., 5.20 vs. 4.94) resulted in a markedly reduced number of nonphysical negative anisotropic R_2 values, suggesting that the proposed gMAE model could considerably improve the characterization of anisotropic R_2 of human knee femoral cartilage on a curved surface.

4 | DISCUSSION

In the current study, a generalized orientation-dependence $f(\alpha, \varepsilon)$ function for anisotropic R_2 relaxation is proposed for better characterization of the MAE in human knee femoral cartilage that has an irregular surface. The proposed gMAE model was first evaluated by simulations then demonstrated on an adult volunteer's asymptomatic knee. Compared with the conventional sMAE functions, the proposed gMAE model provides a significantly improved explanatory power to account for anisotropic T2W signals both in the DZ and in the SZ, and thus a less biased REF could be derived, from which a more reliable anisotropic R_2 relaxation metric could be determined from a single T2W image.

The theoretical framework presented in this work is not particularly different from what was shown in 1962 by Berendsen in his seminal paper.[9] However, the orientation-dependence functional form $f(\alpha, \varepsilon)$ given by Equation 1 sheds more light on the underlying axially symmetric model compared with his original expanded function, which merely provides the same results. Not only does the proposed $f(\alpha, \varepsilon)$ clearly show the multitude symmetries, but it also predicts that the MA (i.e., 54.7°) magically disappears when $\alpha \neq 0°$; in other words, $f(\alpha, \varepsilon)$ can be zero only when $\alpha = 0°$. This interesting finding could be significant when considering a REF derived from the MA orientations.[20] The data listed in Table 1 show that only three out of six fitted α in the DZ were zero; in fact, considering all segmented sagittal slices ($n = 26$), there would be more than 70% of the nonzero-fitted α angles in the DZ (data not shown).

For clinical T2W imaging of human knee articular cartilage at 3 T, an attainable imaging resolution is obviously less than what could be measured ex vivo using μMRI; for instance, the acquired in-plane resolution in this work was 600 x 600 μm^2 with a slice thickness of 3 mm, in contrast to 26 x 13 μm^2 with a slice thickness of 1 mm, as previously reported.[26] Although intrinsically complex, the depth-dependent collagen fibril microstructures studied by clinical T2W imaging at 3 T might be adequately described using a simple analytical function $f(\alpha, \varepsilon)$, which has been proposed herein. It is worthwhile to point out that $f(\alpha, \varepsilon)$ is just an analytical function for the previously mentioned funnel model.[26]

Referred to as a REF in the literature,[20] the fitted model parameter A typically encoded information about nonbound water proton density and isotropic T_2 and T_1 (but not anisotropic T_2) relaxation effects. This particular model parameter is directly linked to an anisotropic R_2, that is, $R_2^a f(\alpha,\varepsilon) = (A - logS)/TE$, derived from a single T2W image using the previously developed ARCADE method[20]; thereby, an underestimated A would be translated into a reduced anisotropic R_2 that could become a negative value. When $\alpha \neq 0$, as in most cases in the femoral cartilage, the highest segmented T2W signals in the DZ, originally thought to be from the MA locations, would most likely contain the contributions from an anisotropic R_2 because of nonzero $f(\alpha, \varepsilon)$. As a result, the REF derived from the conventional approach was noticeably reduced (Figure 7B), resulting in a relatively increased number of negative anisotropic R_2, as shown in Figure 7E,F. It should be noted that the REF from the gMAE model was slightly smaller in the DZ than that in the SZ (i.e., 5.092 ± 0.369 vs. 5.305 ± 0.440). Although this REF difference was small (i.e., about 6%), it was indeed significant ($p = .014$), in good agreement with previous findings.[37–39]

As predicted by the gMAE model (Figure 3B), the dynamic range of $f(\alpha, \varepsilon)$ depends significantly on a particular fibril microstructural configuration (i.e., α). For example, slice 29 (Figures 4B and 6C) cut through an edge of the LFC, presenting a greater MAE variation in the SZ than that in the DZ. This interesting observation could not be explained by the sMAE model that has been commonly used in the preclinical studies on T_2 orientation anisotropy. In those experimental studies, the cartilage surface normal vector direction ($\vec{n}$) was always carefully positioned so that the MAE could become maximized (i.e., $\vec{n} \parallel B_0$).

Surprisingly, Mosher et al. also reported a similar result to that observed for slice 29 in this work, calling into question the validity of the (standard) MAE in the femoral cartilage.[24] It was not surprising that this unexpected finding led to a heated debate among researchers,[40–42] one group of whom had correctly predicted that the curved cartilage surface was responsible for the seemingly contradictory result.[42] The current study actually provides the necessary theoretical framework for adequately understanding the complex nature of anisotropic R_2 of human knee femoral cartilage. With this developed model, it is not difficult to comprehend the previous findings that some R_2 or $R_{1\rho}$ values in the femoral SZ cartilage became even higher than those found in the corresponding DZ.[23,43]

In biological tissues, highly structured macromolecules and their assemblies are ubiquitous; thereby, water proton anisotropic R_2 relaxation becomes a commonplace phenomenon in MR imaging of these highly ordered tissues.[1,44] When interpreting the orientation-dependent transverse relaxation effect originating from a specific highly organized tissue such as human brain white matter, MAE should neither be linked exclusively to the content of collagen, nor should the residual dipolar interactions be considered as orientating in the same direction (i.e., $\alpha = 0$).[45] The proposed gMAE model could possibly find a wide variety of applications in quantifying orientation-dependent R_2 relaxation in highly ordered tissues beyond human knee articular cartilage.

It should be mentioned that some limitations exist in this study. First, the orientation information about an angle ε was heavily dependent on the manual segmentation's accuracy of the femoral cartilage. One of the confounding factors would be a poorly defined cartilage-bone interface. In principle, the developed advanced MR imaging methods such as diffusion and susceptibility tensor imaging techniques[46,47] could provide more accurate collagen fibril orientation information, albeit at the cost of scanning times and the efforts involved in image post-processing. Second, human knee articular cartilage network microstructures are age-dependent,[30] while the femoral cartilage studied in this work was from an adult subject's knee. It thus remains unclear whether or not the proposed gMAE model will be applicable to younger subjects with underdeveloped cartilage microarchitectures. Third, the articular cartilage three-dimensional microstructures are extremely complex, varying across different layers, particularly in the SZ, where two distinct anisotropic components have been previously reported.[26] Hence, it should not be surprising that the proposed gMAE model sometimes does not fit well with the segmented femoral cartilage. Finally, although the isotropic chemical exchange effect has not been considered in this work, it still contributed less than 4% to R_2 in cartilage at 3 T.[20,48] Towards the MA locations, this specific contribution would be increasingly important because the dominant dipolar interactions become increasingly close to zero. Therefore, the determined REF was slightly underestimated at 3 T, and this confounding effect would be exacerbated at higher B_0 fields.

5 | CONCLUSIONS

A general form of the MAE function has been proposed and demonstrated for better characterization of the anisotropic T2W signals from human knee femoral cartilage. Consequently, a more reliable internal reference could be determined, leading to more accurate collagen-specific anisotropic R_2 relaxation rates derived efficiently from a single T2W image. The potential applications of the proposed generalized MAE model could be extended to other highly organized biological tissues, even although the current work focused on cartilage.

ACKNOWLEDGEMENTS

We would like to thank Suzan Lowe and James O'Connor for help in collecting the human knee cartilage images. This work was in part supported by the Eunice Kennedy Shriver National Institute of Child Health & Human Development of the National Institutes of Health (NIH) under Award Number 5-R01-HD-093626-02 (to Prof. Riann Palmieri-Smith). The content is solely the responsibility of the author and does not necessarily represent the official views of the NIH.

ORCID

Yuxi Pang https://orcid.org/0000-0001-5039-0236

REFERENCES

1. Bydder M, Rahal A, Fullerton GD, Bydder GM. The magic angle effect: A source of artifact, determinant of image contrast, and technique for imaging. *J Magn Reson Imaging*. 2007;25(2):290-300. https://doi.org/10.1002/jmri.20850
2. Fullerton GD. The magic angle effect in NMR and MRI of cartilage. In: Xia Y, Momot KI, eds. *Biophysics and Biochemistry of Cartilage by NMR and MRI*. Cambridge, UK: The Royal Society of Chemistry; 2016:109-144. https://doi.org/10.1039/9781782623663-00109
3. Xia Y. Magic-angle effect in magnetic resonance imaging of articular cartilage: a review. *Invest Radiol*. 2000;35(10):602-621.
4. Hanninen N, Rautiainen J, Rieppo L, Saarakkala S, Nissi MJ. Orientation anisotropy of quantitative MRI relaxation parameters in ordered tissue. *Sci Rep*. 2017;7(1):1-11.
5. Pang Y. An order parameter without magic angle effect (OPTIMA) derived from R1ρ dispersion in ordered tissue. *Magn Reson Med*. 2020;83(5):1783-1795.
6. Fullerton GD, Rahal A. Collagen structure: The molecular source of the tendon magic angle effect. *J Magn Reson Imaging*. 2007;25(2):345-361. https://doi.org/10.1002/jmri.20808
7. Tourell MC, Momot KI. Molecular Dynamics of a Hydrated Collagen Peptide: Insights into Rotational Motion and Residence Times of Single-Water Bridges in Collagen. *J Phys Chem B*. 2016;120(49):12432-12443. https://doi.org/10.1021/acs.jpcb.6b08499
8. Erickson SJ, Prost RW, Timins ME. The "magic angle" effect: background physics and clinical relevance.. *Radiology*. 1993;188(1):23-25. https://doi.org/10.1148/radiology.188.1.7685531
9. Berendsen HJC. Nuclear magnetic resonance study of collagen hydration. *J Chem Phys*. 1962;36(12):3297-3305.
10. Momot KI, Pope JM, Wellard RM. Anisotropy of spin relaxation of water protons in cartilage and tendon. *NMR Biomed*. 2010;23(3):313-324. https://doi.org/10.1002/nbm.1466
11. Bella J. Collagen structure: new tricks from a very old dog. *Biochem J*. 2016;473(8):1001-1025. https://doi.org/10.1042/bj20151169
12. Woessner DE. Nuclear magnetic-relaxation and structure in aqueous heterogenous systems. *Mol Phys*. 1977;34(4):899-920.
13. Totland C, Nerdal W. Experimental Determination of Water Molecular Orientation near a Silica Surface Using NMR Spectroscopy. *J Phys Chem C*. 2016;120(9):5052-5058. https://doi.org/10.1021/acs.jpcc.6b00466
14. Fung B. Orientation of water in striated frog muscle. *Science*. 1975;190(4216):800-802.
15. Peto S, Gillis P, Henri VP. Structure and dynamics of water in tendon from NMR relaxation measurements. *Biophys J*. 1990;57(1):71-84. https://doi.org/10.1016/s0006-3495(90)82508-x
16. Lenk R, Bonzon M, Greppin H. Dynamically oriented biological water as studied by NMR. *Chem Phy Lett*. 1980;76(1):175-177.
17. Link TM, Neumann J, Li X. Prestructural cartilage assessment using MRI. *J Magn Reson Imaging*. 2017;45(4):949-965. https://doi.org/10.1002/jmri.25554
18. Roemer FW, Kijowski R, Guermazi A. Editorial: from theory to practice - the challenges of compositional MRI in osteoarthritis research. *Osteoarthr Cartil*. 2017;25(12):1923-1925.
19. Link TM, Li X. Establishing compositional MRI of cartilage as a biomarker for clinical practice. *Osteoarthr Cartil*. 2018;26(9):1137-1139.
20. Pang Y, Palmieri-Smith RM, Malyarenko DI, Swanson SD, Chenevert TL. A unique anisotropic R2 of collagen degeneration (ARCADE) mapping as an efficient alternative to composite relaxation metric (R2 -R1 rho) in human knee cartilage study. *Magn Reson Med*. 2019;81(6):3763-3774.
21. Monk AP, Choji K, O'Connor JJ, Goodfellow† JW, Murray DW. The shape of the distal femur. *Bone Joint J*. 2014;96-B(12):1623-1630. https://doi.org/10.1302/0301-620x.96b12.33964
22. Morales Martinez A, Caliva F, Flament I, et al. Learning osteoarthritis imaging biomarkers from bone surface spherical encoding. *Magn Reson Med*. 2020;84(4):2190-2203. https://doi.org/10.1002/mrm.28251
23. Kaneko Y, Nozaki T, Yu H, et al. Normal T2 map profile of the entire femoral cartilage using an angle/layer-dependent approach. *J Magn Reson Imaging*. 2015;42(6):1507-1516. https://doi.org/10.1002/jmri.24936
24. Mosher TJ, Smith H, Dardzinski BJ, Schmithorst VJ, Smith MB. MR imaging and T2 mapping of femoral cartilage: in vivo determination of the magic angle effect. *Am J Roentgenol*. 2001;177(3):665-669. https://doi.org/10.2214/ajr.177.3.1770665
25. Jeffery AK, Blunn GW, Archer CW, Bentley G. Three-dimensional collagen architecture in bovine articular cartilage. *J Bone Joint Surg. British volume*. 1991;73-B(5):795-801. https://doi.org/10.1302/0301-620x.73b5.1894669
26. Zheng S, Xia Y, Badar F. Further studies on the anisotropic distribution of collagen in articular cartilage by μMRI. *Magn Reson Med*. 2011;65(3):656-663.
27. Garnov N, Gründer W, Thörmer G, et al. In vivo MRI analysis of depth-dependent ultrastructure in human knee cartilage at 7 T. *NMR Biomed*. 2013;26(11):1412-1419. https://doi.org/10.1002/nbm.2968
28. Mlynárik V, Degrassi A, Toffanin R, Vittur F, Cova M, Pozzi-Mucelli RS. Investigation of laminar appearance of articular cartilage by means of magnetic resonance microscopy. *Magn Reson Imaging*. 1996;14(4):435-442. https://doi.org/10.1016/0730-725x(96)00025-2
29. Xia Y. Relaxation anisotropy in cartilage by NMR microscopy (muMRI) at 14-microm resolution. *Magn Reson Med*. 1998;39(6):941-949.
30. Grunder W. MRI assessment of cartilage ultrastructure. *NMR Biomed*. 2006;19(7):855-876.

31. Benninghoff A. Form und Bau der gelenkknorpel in ihren Beziehungen zur funktion-Erste Mitteilung: Die modellierenden und formerhaltenden Faktoren des Knorpelreliefs. *Zeitsh f Anatomie*. 1925;76:43-63.
32. Hennel JW, Klinowski J. Magic-angle spinning: a historical perspective. In: Klinowski J, ed. *New Techniques in Solid-State NMR*. Berlin, Heidelberg, Germany: Springer; 2005;1-14.
33. Geerts-Ossevoort L, Weerdt Ed, Duijndam A, et al. Compressed SENSE. Speed done right. Every time. https://philipsproductcontent.blob.core.windows.net/assets/20180109/619119731f2a42c4acd4a863008a46c7.pdf. 2018; Accessed September 20, 2019.
34. Yushkevich PA, Piven J, Hazlett HC, et al. User-guided 3D active contour segmentation of anatomical structures: significantly improved efficiency and reliability. *Neuroimage*. 2006;31(3):1116-1128. https://doi.org/10.1016/j.neuroimage.2006.01.015
35. Markwardt CB. Non-linear least-squares fitting in IDL with MPFIT. In: Bohlender D, Dowler P, Durand D, eds. *Proceedings Astronomical Data Analysis Software and Systems XVIII, Quebec, Canada, ASP Conference Series, volume 411*. San Francisco, CA: Astronomical Society of the Pacific; 2009:251-254.
36. Ahearn TS, Staff RT, Redpath TW, Semple SIK. The use of the Levenberg–Marquardt curve-fitting algorithm in pharmacokinetic modelling of DCE-MRI data. *Phys Med Biol*. 2005;50(9):N85-N92.
37. Shapiro E, Borthakur A, Kaufman J, Leigh J, Reddy R. Water distribution patterns inside bovine articular cartilage as visualized by1H magnetic resonance imaging. *Osteoarthr Cartil*. 2001;9(6):533-538.
38. Berberat JE, Nissi MJ, Jurvelin JS, Nieminen MT. Assessment of interstitial water content of articular cartilage with T1 relaxation. *Magn Reson Imaging*. 2009;27(5):727-732. https://doi.org/10.1016/j.mri.2008.09.005
39. Xia Y. MRI of articular cartilage at microscopic resolution. *Bone Joint Res*. 2013;2(1):9-17. https://doi.org/10.1302/2046-3758.21.2000135
40. Xia Y, Moody JB, Alhadlaq H. Orientational dependence of T2 relaxation in articular cartilage: A microscopic MRI (microMRI) study. *Magn Reson Med*. 2002;48(3):460-469. https://doi.org/10.1002/mrm.10216
41. Mlynárik V. Magic angle effect in articular cartilage. *Am J Roentgenol*. 2002;178(5):1287-1288. https://doi.org/10.2214/ajr.178.5.1781287
42. Goodwin DW, Dunn JF. MR imaging and T2 mapping of femoral cartilage. *Am J Roentgenol*. 2002;178(6):1568-1569.
43. Nozaki T, Kaneko Y, Hon JY, et al. T1rho mapping of entire femoral cartilage using depth-and angle-dependent analysis. *Eur Radiol*. 2016;26(6):1952-1962.
44. Henkelman RM, Stanisz GJ, Kim JK, Bronskill MJ. Anisotropy of NMR properties of tissues. *Magn Reson Med*. 1994;32(5):592-601.
45. Pang Y. Anisotropic transverse relaxation in the human brain white matter induced by restricted rotational diffusion. In: Proceedings of the 29th Virtual Annual Meeting of ISMRM, 2021; abstract: 1711.
46. Wang N, Mirando AJ, Cofer G, Qi Y, Hilton MJ, Johnson GA. Characterization complex collagen fiber architecture in knee joint using high-resolution diffusion imaging. *Magn Reson Med*. 2020;84(2):908-919. https://doi.org/10.1002/mrm.28181
47. Wei H, Gibbs E, Zhao P, et al. Susceptibility tensor imaging and tractography of collagen fibrils in the articular cartilage. *Magn Reson Med*. 2017;78(5):1683-1690.
48. Mlynarik V, Szomolanyi P, Toffanin R, Vittur F, Trattnig S. Transverse relaxation mechanisms in articular cartilage. *J Magn Reson*. 2004;169(2):300-307.

How to cite this article: Pang Y. Characterization of anisotropic T2W signals from human knee femoral cartilage: The magic angle effect on a spherical surface. *NMR in Biomedicine*. 2021;34:e4535. https://doi.org/10.1002/nbm.4535